Key predictors of earthquake-induced lateral spreading in liquefiable slopes

Masoumeh Asgarpoor, Andrés Reyes & Mahdi Taiebat
Department of Civil Engineering – University of British Columbia, Vancouver, BC, Canada

GeoCalgary 2022 October 2-5 Reflection on Resources

ABSTRACT
Mildly sloped liquefiable sand deposits are susceptible to lateral spreading under earthquake ground motion. Geometry, material properties, and input motion are the high-level impacting factors on the slope displacements. The recently developed SANISAND-MSf, a two-surface sand plasticity model with memory surface and semifluidized state, is used in the finite difference-based platform *FLAC3D* to simulate the nonlinear behavior of the soil. A multi-layer system with different thicknesses of liquefiable layer, various sand relative densities, and a suite of ground motion intensities are considered to study the primary design variables affecting the slope response. The simulation results indicate that superficial lateral displacements increase significantly with increasing thickness of the liquefiable layer, decreasing relative density, and increasing cumulative absolute velocity of the ground motion. Furthermore, the lateral spreading obtained under bidirectional shaking may be smaller or larger than that under unidirectional, highlighting the importance of accounting for the former in predicting the response of liquefiable slopes.

RÉSUMÉ
Les dépôts de sable liquéfiable légèrement inclinés sont susceptibles de se propager latéralement sous le mouvement du sol sismique. La géométrie, les propriétés des matériaux et le mouvement d'entrée sont les facteurs d'impact de haut niveau sur les déplacements de pente. Le SANISAND-MSf récemment développé, un modèle de plasticité du sable à deux surfaces avec surface mémoire et état semi-fluidisé, est utilisé dans la plate-forme basée sur les différences finies FLAC3D pour simuler le comportement non linéaire du sol. Un système multicouche avec différentes épaisseurs de couche liquéfiable, diverses densités relatives de sable et une suite d'intensités de mouvement du sol sont considérés pour étudier la principale variable de conception affectant la réponse de la pente. Les résultats de la simulation indiquent que les déplacements latéraux superficiels augmentent de manière significative avec l'augmentation de l'épaisseur de la couche liquéfiable, la diminution de la densité relative et l'augmentation de la vitesse absolue cumulative du mouvement du sol. De plus, l'étalement latéral obtenu sous agitation bidirectionnelle peut être plus petit ou plus grand que celui sous unidirectionnel, soulignant l'importance de tenir compte du premier pour prédire la réponse des pentes liquéfiables.

1 INTRODUCTION

The surface displacements caused by earthquake-induced liquefaction in inclined granular deposits are typically referred to as lateral spreading. This type of ground deformation constitutes a potentially destructive phenomenon that can affect buildings, lifelines, and other engineered structures (Barlett and Youd, 1995). During the seismic shearing, mean cyclic shear stress (τ_{mean}), or the so-called initial shear stress, is also imposed on these deposits due to their inclined nature. The combination of cyclic shear stresses (τ_{cyc}) and τ_{mean} is the driving mechanism behind the progressive accumulation of cyclic shear strains along the dip direction of the slope during the seismic loading, which in turn results in large surface displacements observed at the end of shaking.

Empirical methods, physical modeling, and numerical simulations are usually employed to study and predict lateral spreading. Most empirical regression equations, such as those proposed by Bardet et al. (1999) and Youd et al. (2002), rely on observations from liquefaction case histories and associate surface displacements to the geotechnical and seismological parameters. Since the inception of the Verification of Liquefaction Analyses and Centrifuge Studies, or VELACS (Arulanandan and Scott, 1993), physical modeling has been extensively used to study lateral spreading. The next major study in this direction was the Canadian Liquefaction Experiment, or CANLEX (Robertson et al., 2000). Most recently, the Liquefaction Experiments and Analysis Projects, or LEAP (Kutter et al., 2018, 2020), have produced a wealth of element level and centrifuge experimental data designed to study the lateral spreading of mildly sloped liquefiable soil deposits. These centrifuge tests have also been used to validate and improve constitutive models for sands, which in turn are used to study lateral spreading. Elgamal et al. (2002) used the results from selected VELACS centrifuge tests and highlighted the effect of the frequency content of shaking on the resulting ground displacements. Valsamis et al. (2010) used a validated numerical modeling approach to associate the lateral spreading of a gently sloping ground with its inclination, characteristics of the shaking, and soil cyclic strength. Similarly, the effect of geometric and seismic parameters on the resulting lateral spreading of liquefiable slopes was investigated by Ghasemi-Fare and Pak (2016). More recently, the sensitivity of the lateral spreading of liquefiable slopes to the variability of soil density and base excitation was investigated by El Ghoraiby and Manzari (2020).

The main objective of this paper is to study the effects of the thickness and depth of the liquefiable layer, soil relative density, and ground motion intensity on the lateral spreading of a mildly inclined infinite slope. For this purpose, a validated pair of constitutive model and numerical modeling approach is used to simulate a layered soil column subjected to uni- and bidirectional seismic shearing. A parametric analysis is then conducted, varying the model geometry, soil initial void ratio, and input motion. The results are summarized by assessing how impactful the changes in geometry, material properties, and nature of the ground motion are for predicting lateral spreading.

2 SOIL CONSTITUTIVE MODEL

Dafalias and Manzari (2004) introduced a stress-ratio controlled, critical state compatible, bounding surface plasticity model, often referred to as DM04, which formed the basis of what was later named the SANISAND class of models (Taiebat and Dafalias, 2008). The DM04 model is well established as it has been widely used over the years for a variety of liquefaction related problems. The SANISAND class includes various extensions, each addressing different aspects of the mechanical response of sands. With respect to undrained cyclic shearing, two major limitations of the DM04 constitutive model have been identified: i) the lack of adequate control of the pre-liquefaction plastic stiffness for a wide range of cyclic shear stresses, and ii) the limited modeling of large post-liquefaction shear strains. To address these shortcomings, Yang et al. (2022) proposed two new constitutive ingredients which suggested the name SANISAND-MSf (S-MSf) for the model, with M standing for 'memory surface' and Sf for 'semifluidised state'. The memory surface was formulated to accurately control the plastic stiffness in pre-liquefaction. This memory surface is a back-stress-ratio based bounding surface with kinematic and isotropic hardening. A normalized measure of the distance between memory surface and stress-ratio is used to affect the plastic modulus within DM04, which in turn allows for an improved control on the rate of plastic deviatoric and volumetric strains in pre-liquefaction. The impact of the memory surface on the plastic modulus is regulated with the introduction of model constants μ_0 and u. The concept of a semifluidized state is employed to degrade the plastic stiffness and dilatancy of the model in order to simulate the progressive development of large cyclic shear strains in post-liquefaction. The Sf state was proposed by Barrero et al. (2020), who postulated a new internal variable I that evolves at very low values of mean effective stress p. The plastic modulus and dilatancy in DM04 are simultaneously degraded through I, granting the means to model increasing plastic shear strains in post-liquefaction without impacting the plastic volumetric strains. The degradation is controlled through model constants x and c_I.

In earlier studies the reference SANISAND models were assessed in simulating the propagation of seismic wave through liquefied soils (Taiebat et al. 2010) and validated against centrifuge tests conducted for layered liquefiable soil deposits (Taiebat et al. 2007, Shahir et al. 2012, Tasiopoulou, et al 2015, Ramierez et al. 2016), and liquefiable elements and deposits subjected to bidirectional shearing (Yang et al. 2019, Reyes et al. 2019). For the purposes of this study the predictive capabilities of the S-MSf model have been thoroughly validated against centrifuge tests of submerged liquefiable deposits prone to lateral spreading in Reyes et al. (2021) and Perez et al. (2022). Table 1 presents model constants of S-MSf calibrated for Ottawa F65 sand from hollow cylinder cyclic torsional shear tests by Vargas et al. (2020).

Table 1. SANISAND-MSf calibrated model constants

Description	Symbol	Ottawa F65 sand
Elasticity	G_0	125
	υ	0.05
Critical state	M^c	1.26
	c	0.735
	e_c^{ref}	0.78
	λ_c	0.0287
	ξ	0.7
Yield surface	m	0.01
Kinematic hardening	n^b	3.5
	h_0'	4.6
	c_h	0.968
Dilatancy	n^d	2.5
	A_0'	0.626
	n_g	0.9
Fabric dilatancy	$z_{\max}$	15
	c_z	2000
Memory surface	μ_0	1.99
	u	1.32
Semifluidized state	x	3.5
	c_I	35

3 NUMERICAL MODEL DESCRIPTION

The numerical simulations were conducted in the finite difference platform *FLAC3D* v7 (Itasca, 2021), which solves the dynamic equation of motion using an explicit time-integration method and allows for coupled solid-pore fluid interaction calculations. The S-MSf model is implemented in *FLAC3D* using a semi-explicit integration scheme.

The numerical model employed to represent the infinite slope was a 10-m vertical soil column consisting of 20 eight-node brick elements (0.5 × 0.5 × 0.5m), as shown in the schematic 3D view of Figure 1a. The infinite slope conditions are modeled i) using horizontal and vertical gravity components computed from the angle of the sloping ground, and ii) tying the lateral nodes of the brick elements at each depth. Furthermore, during the dynamic stage of the analysis, the seismic shearing is propagated along the vertical axis of the soil column. The model was constructed sequentially, starting by considering a linear elastic soil model and stabilized to reach initial conditions before the dynamic stage. A water table with a depth of 1m was considered. To model the solid-pore fluid interaction, the built-in isotropic fluid model was used with a water bulk modulus of 2.0×10^6 kPa and hydraulic conductivity of 0.01 cm/s. After generating the initial pore water pressures, the soil constitutive model changed to S-MSf. In the dynamic

stage, seismic loading is applied at the bottom nodes by freeing the horizontal degrees of freedom.

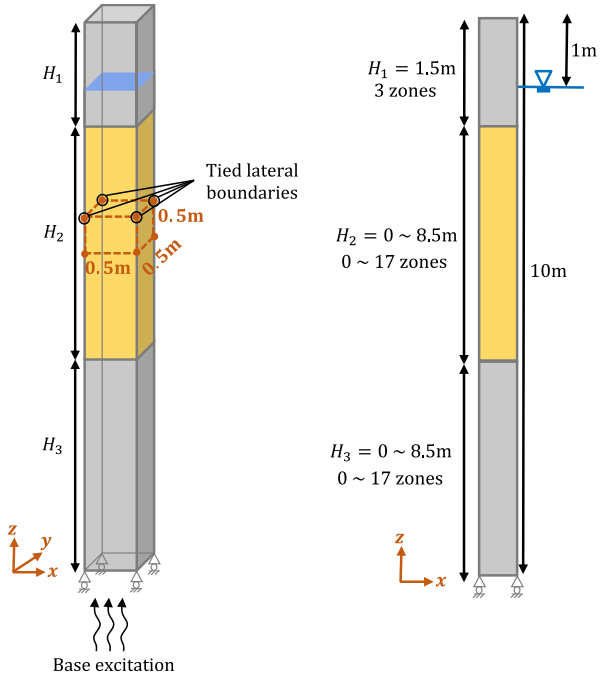

(a) Soil column model (b) Soil layering

Figure 1. Soil column model and illustration of layering

For the parametric study, several scenarios are studied. First, the geometry of the deposit is varied in terms of its layering and inclination. Three soil layers are considered in the soil column model, as depicted in Figure 1b. A top crust with a constant thickness H_1 = 1.5m and D_r = 90% is used in all analyses. The thickness of middle layer H_2 is varied from 0 to 8m. The thickness of the bottom layer H_3, with D_r = 90%, varies depending on H_2. Three slope angles of 1, 4, and 7 degrees are also considered. Ottawa F65 sand is considered in all analyses with S-MSf model constants provided in Table 1. Maximum and minimum void ratios of Ottawa F-65 considered for calculation of the relative densities are 0.777 and 0.508, respectively.

Second, to evaluate the impact of the initial void ratio, four relative densities of 40, 55, 70 and 90% are used for the middle layer. Third, four ground motions are considered for the analyses. For each ground motion, both unidirectional (UD) and bidirectional (BD) shearing are used as excitations. The UD shearing analysis employs the horizontal component with the highest cumulative absolute velocity (CAV), which is applied in the *x* direction, i.e., along the dip direction of the slope. For BD shearing, the corresponding orthogonal component is applied simultaneously in the *y* direction. Table 2 summarizes relevant characteristics of the ground motion, and Figure 2 shows the acceleration time-histories corresponding to the *x* direction. The summary of scenarios considered for the parametric analyses are provided in Table 3. To study the effect of each parameter, a constant value is assumed for the other parameters, referred to as reference values in Table 3.

Table 2. Ground motion characteristics

Ground motion	Dur. (s)	M_w	Dir.	CAV (m/s)	PGA (g)
EQ1 (Kobe,1995)	40	6.9	*x*	3.63	0.22
			y	3.43	0.23
EQ2 (El Centro,1987)	60	6.5	*x*	5.63	0.36
			y	5.19	0.26
EQ3 (Loma Prieta,1989)	40	6.9	*x*	8.94	0.51
			y	6.85	0.44
EQ4 (Imperial Vly,1979)	100	6.5	*x*	14.44	0.35
			y	12.69	0.24

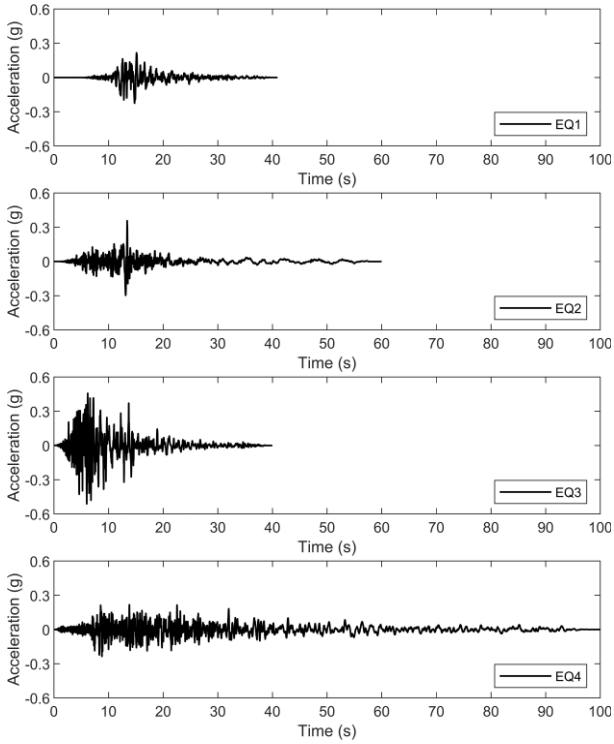

Figure 2. Acceleration time histories of ground motion horizontal components used as input in the *x* direction

4 PARAMETRIC STUDY

4.1 Thickness of middle layer

Figure 3 shows the lateral displacement in depth for different thicknesses of the middle layer. The case of H_2 = 0m results in a homogeneous soil column with D_r = 90% and shows the lowest level of deformation. Increasing H_2 results in larger lateral displacements, as expected. Furthermore, the lateral displacements are larger under UD shearing than under BD shearing, regardless of the thickness of the middle layer.

Table 3. Input parameters for numerical parametric study

Input Parameter (IP)	Value of IP	Reference value
Thickness of middle layer (H_2)	0, 2, 6, 8m	4m
Slope inclination	1, 4, 7 degrees	4 degrees
D_r of middle layer	40, 55, 70, 90%	55%
Ground motion	EQ1, EQ2, EQ3, EQ4	EQ1

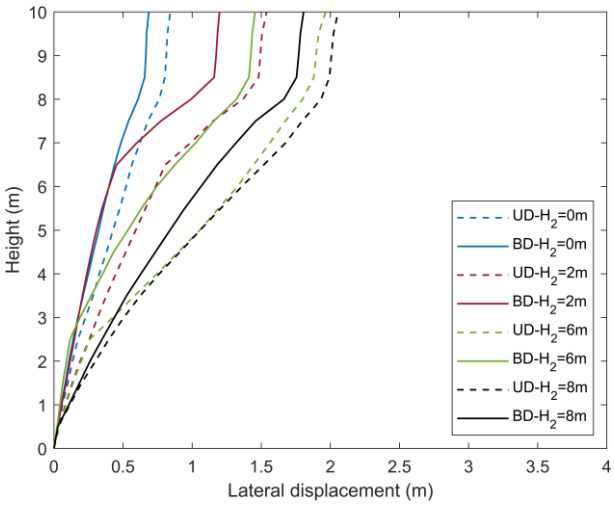

Figure 3. Lateral displacement in depth with changing thickness of liquefiable layer

4.2 Slope angle

The effect of slope inclination on lateral displacement of liquefiable slopes is evaluated in Figure 4. Horizontal dashed lines at depths 1.5m and 8.5m show the boundaries between crust, middle layer, and dense sand at the bottom. Here, a distinction must be made between the UD and BD shearing scenarios. Under UD shearing, it can be observed that increasing the slope inclination leads to a steady increase of lateral displacements. However, under the more realistic BD shearing, this trend is reversed. In fact, the observations made for UD and BD shearing in section 4.1, where displacements in BD shearing are smaller, hold true only for inclinations of 4 and 7 degrees. For the case of 1 degree, the simulations indicate that the results for BD shearing are larger than those obtained in UD shearing.

For further insight, mean effective stress time histories at different heights of the soil columns with slope angles of 1 and 7 degrees are presented in Figures 5 and 6, respectively. Reaching a state of mean effective of stress of zero for the first time is referred to as initial liquefaction. Considering this, Figure 5 shows that a state of liquefaction is reached for the UD shearing case starting from a height of 4.75m, which is then reflected by the negligible lateral displacements obtained until this height in Figure 4. On the other hand, liquefaction is reached from a much lower height for the BD shearing case, resulting in larger lateral displacements.

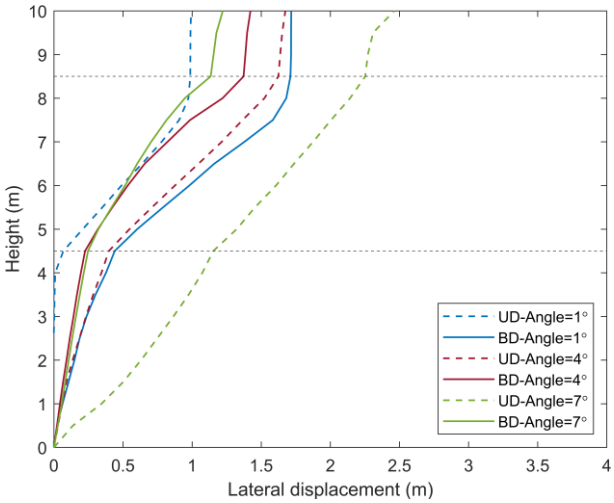

Figure 4. Lateral displacement in depth with changing slope angle

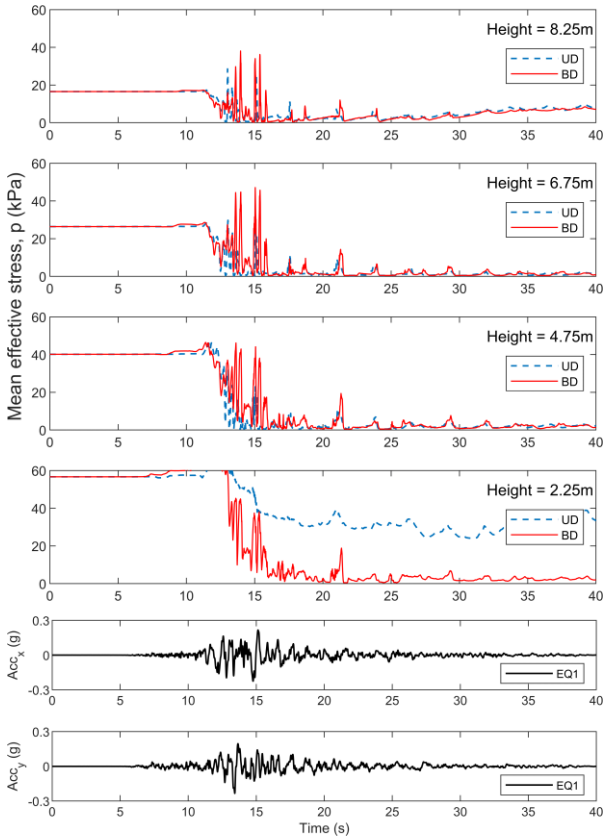

Figure 5. Mean effective stress time histories at different heights for the soil column with slope angle of 1 degree. Acceleration time histories used as base input are shown at the bottom.

Figure 6 shows a similar profile of mean pressure time histories for the soil column with slope angle of 7 degree. For this case both UD and BD shearing result in initial liquefaction starting from a height of 2.25m. For the UD shearing, this fact explains the larger displacements obtained the more inclined the slope column is. However, unlike the results show for a slope angle of 1 degree, the state of mean effective stress of zero is not maintained throughout shaking. This is likely due to the higher values of τ_{mean} present in the latter case, which results in preventing as many scenarios of zero mean effective stresses during shaking than in former. It is suggested then that the effect of τ_{mean} combined with the nature of BD shearing results is less displacements that their UD shearing counterparts.

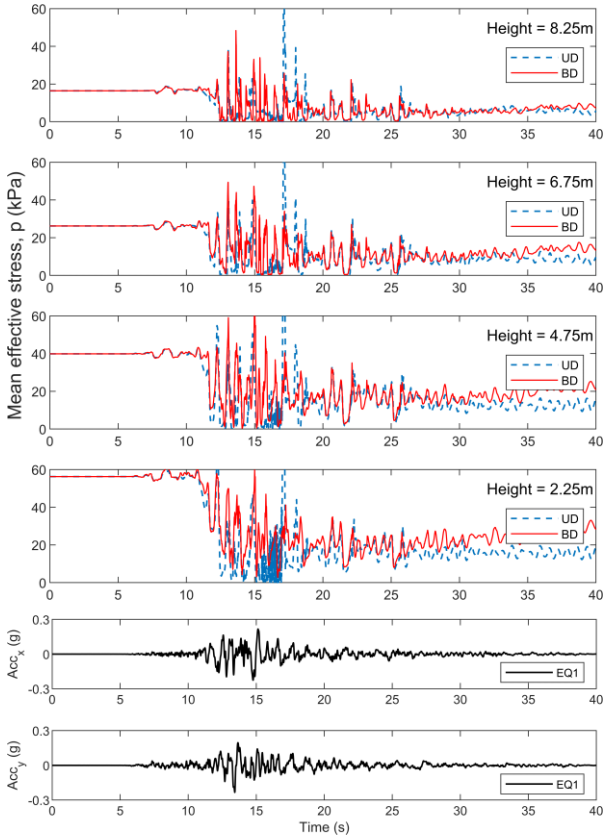

Figure 6. Mean effective stress time histories at different heights for the soil column with slope angle of 7 degrees. Acceleration time histories used as base input are shown at the bottom

4.3 Relative density

The effect of initial void ratio of the middle layer on the end of shaking lateral displacements is shown in Figure 7. As expected, the displacements obtained decrease as the relative density increases. This is consistent with experimental observations that indicate that cyclic resistance increases with increasing relative density. Note that obtaining larger displacements for looser middle layers occurs when subjected to either UD or BD shearing. Furthermore, as in section 4.1, the lateral displacements are lower during BD shearing.

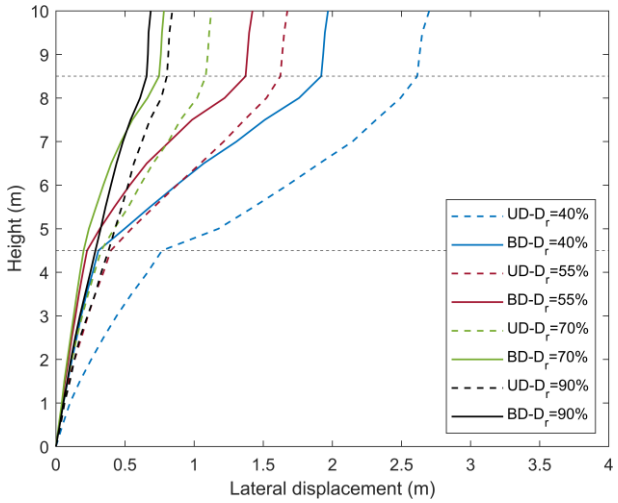

Figure 7. Lateral displacement in depth for different relative densities of middle layer

4.4 Ground motion intensity

Four ground motion records with the characteristics provided in Table 2 and time histories shown in Figure 2 are applied to the numerical model. The effect of ground motion intensity on lateral displacement of soil column is presented in Figure 8, which shows that the obtained lateral spreading is proportional to the CAV intensities of the base excitations, where EQ1 to EQ4 have increasing values of CAV. Note that while EQ4 has a lower PGA than EQ3, it has a much longer duration, which results in a higher CAV value. Moreover, as depicted in sections 4.1 and 4.3, lateral displacements obtained in BD shearing are lower than those resulting in UD shearing.

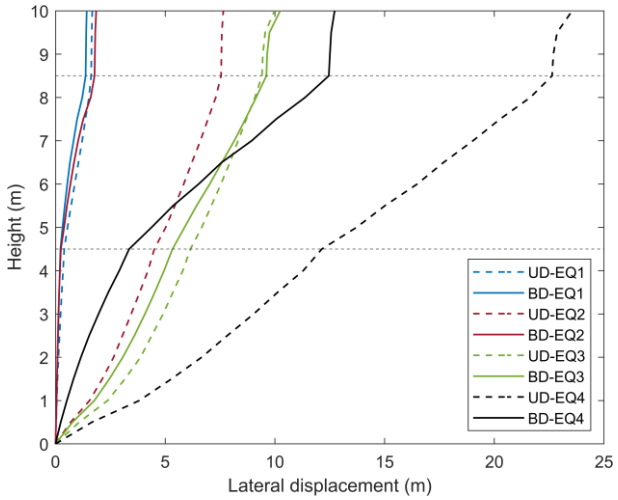

Figure 8. Lateral displacement in depth with different base excitations

4.5 Summary of results

The parametric study presented here indicates that lateral displacements of a liquefiable soil deposit increase with increasing thickness or decreasing relative density of the middle layer, and with larger CAV of the input ground motion. These statements are shown to be valid for both UD and BD seismic shearing. Moreover, it is shown that for these scenarios, the displacements obtained in BD shearing are smaller than those in UD shearing. However, when varying the inclination of the slope from 1 to 7 degrees, different observations are made from the UD and BD shearing cases. Why does this happen? Three factors must be addressed. First, it is relevant to review which are the mechanisms of deformation that occur after reaching the state of liquefaction. When cross-over occurs, i.e., shear stress component in one direction changes its sign, deformation occurs due to cyclic liquefaction. In S-MSf, the semifluidized state formulation allows for the modeling of large shear deformations associated with cyclic liquefaction. However, in the absence of cross-over during cyclic loading, cyclic deformations accumulate slower. These much smaller deformations are modeled in S-MSf primarily through the bounding and memory surface formulations. Consequently, it is expected that after initial liquefaction, the larger occurrence of cross-over instances during shearing, the larger the deformation will be. Second, what causes instances of cross-over? In general, the combination of τ_{mean} and τ_{cyc} will control this occurrence: when $\tau_{\mathrm{mean}} < \tau_{\mathrm{cyc}}$, cross-over will transpire. Third, cyclic strength depends on the level of τ_{mean} and the occurrence of cross-over.

The results for UD shearing in Figure 4, where slope inclination is varied, suggest that increasing the slope angle, which effectively increases τ_{mean}, results in larger displacements. This increase in displacements is likely caused by the decrease of cyclic strength obtained in S-MSf model for small values of τ_{mean}, which are not expected to significantly prevent cross-over during cyclic shearing, and the larger extent of liquefaction in the soil column. However, it appears that in BD shearing cross-over is prevented in more instances than in its corresponding UD shearing case. Figure 9, showing the time-history of the octahedral shear stress (τ_{oct}) in the middle of the soil column for the inclination of 4 degrees and $D_r = 55\%$ is useful to understand this. First, in UD shearing, initial liquefaction occurs the first time τ_{oct} reaches a value of zero at around 12.5 seconds. Subsequent zero values of τ_{oct} reflect the occurrence of cross-over instances. On the other hand, in BD shearing, initial liquefaction occurs at around 14 seconds, and the subsequent instances of cross-over are less numerous than in the UD case. Overall, it can be argued that the presence of τ_{mean}, combined with the shear stress histories induced by BD shearing, can result in fewer instances of cross-over and smaller lateral displacements than for UD shearing cases.

5 CONCLUSIONS

This study presented a numerical parametric study to evaluate key predictors of earthquake-induced lateral spreading in layered, liquefiable, mildly inclined infinite slopes. Using the novel constitutive model SANISAND-MSf implemented in *FLAC3D*, several soil columns which represented the inclined slope were analyzed considering different scenarios of soil type, layering, slope inclination, relative densities and ground motion intensities. The results indicate that superficial lateral displacements increase significantly with increasing thickness of liquefiable layer, decreasing relative density and increasing cumulative absolute velocity of the ground motion. Moreover, in general, the displacements obtained considering shaking under bidirectional loading are smaller than when considering unidirectional shearing, highlighting the importance of accounting bidirectional seismic shearing. The combined effect of mean shear stresses present in the slope and the earthquake-induced cyclic shear stresses is likely responsible for this observation. It is of particular interest to observe that, when considering bidirectional shearing, the displacements of the slope decrease with increasing slope inclination. Properly accounting for the impact of non-zero mean shear stresses in the constitutive model is paramount, as the results suggest that the predicted lateral spreading may depend largely on the simulated cyclic strength and deformation for different combinations of τ_{cyc} and occurrences of cross-over during cyclic shearing.

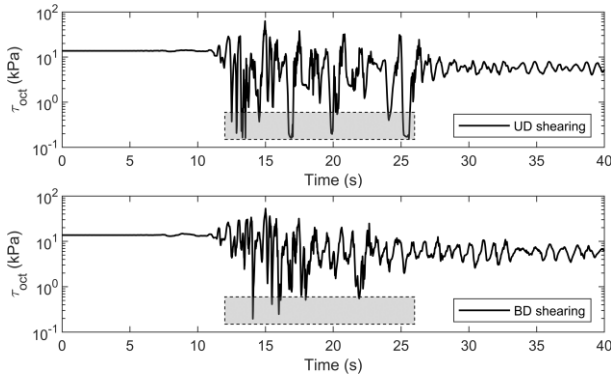

Figure 9. Time histories of octahedral shear stress obtained at the middle of soil column analyzed for the reference case: H_2 = 4m, slope inclination of 4 degrees, $D_{\mathrm{r}} = 55\%$ and using motion EQ1.

ACKNOWLEDGEMENT

Financial support for this study was provided by the Natural Sciences and Engineering Research Council of Canada (NSERC).

REFERENCES

Arulanandan K. and Scott RF. 1993. Verification of numerical procedures for the analysis of soil liquefaction problems, *Arulanandan K. and Scott RF*, Davis, CA, 1.

Bartlett, S.F. and Youd, T.L. 1995. Empirical prediction of liquefaction-induced lateral spread. *Journal of Geotechnical Engineering*, 121(4): 316-329.

Barrero, A.R., Taiebat, M. and Dafalias, Y.F. 2020. Modeling cyclic shearing of sands in the semifluidized state*. International Journal for Numerical and Analytical Methods in Geomechanics*, 44: 371-388.

Bardet, J., Mace, N. and Tobita, T. 1999. Liquefaction-induced ground deformation and failure, a report to PEER/PG&E. Task 4A-Phase 1., Los Angeles: Civil Engineering Department, University of Southern California.

Dafalias YF, Manzari MT. 2004. Simple plasticity sand model accounting for fabric change effects. *Journal of Engineering mechanics*, 130: 622–34.

Elgamal, A., Yang, Z. and Parra, E. 2002. Computational modeling of cyclic mobility and post-liquefaction site response. *Soil Dynamics and Earthquake Engineering*, 22: 259-271.

ElGhoraiby, M.A. and Manzari, M.T. 2020. The effects of base motion variability and soil heterogeneity on lateral spreading of mildly sloping ground. *Soil Dynamics and Earthquake Engineering*, 135: 106185.

Ghasemi-Fare, O. and Pak, A. 2016. Numerical investigation of the effects of geometric and seismic parameters on liquefaction-induced lateral spreading. *Soil Dynamics and Earthquake Engineering*, 89: 233-247.

Itasca. FLAC3D-Fast Lagrangian analysis of Continua in three-dimensions, version 7.0. 2021. Minneapolis, Minnesota: Itasca Consulting Group, Inc.

Kutter, B.L., Carey T.J., Hashimoto, T., Zeghal, M., Abdoun, T.H., Kokkali, P., Madabushi, G., Haigh, S., dArezzo, F.B., Madabushi, S., Hung, W.Y., Lee, C.J., Cheng, H.C., Iai, S., Tobita, T., Ashino, T., Ren, J., Zhou, Y.G., Chen, Y., Sun, Z.B. and Manzari M.T. 2018. LEAP-GWU-2015 experiment specifications, results, and comparisons. *Soil Dynamiics and Earthquake Engineering*, 113:616–28.

Kutter, B.L., Manzari, M.T. and Zeghal, M. 2020. *Model Tests and Numerical Simulations of Liquefaction and Lateral Spreading LEAP-UCD-2017*. Springer, Switzerland.

Perez, K., Reyes, A. and Taiebat, M. 2022. Numerical modeling of the LEAP-RPI-2020 centrifuge tests using SANISAND-MSf. In *Performance-based Design in Earthquake. Geotechnical Engineering (PBD-IV)*, 15-19 July, Beijing, China, (in-press).

Ramirez, J., Barrero, A.R., Chen, L., Dashti, S., Ghofrani, A., Taiebat, M. and Arduino, P. 2018. Site response in a layered liquefiable deposit: evaluation of different numerical tools and methodologies with centrifuge experimental results. *Journal of Geotechnical and Geoenvironmental Engineering*, 144: 04018073.

Reyes, A., Adinata, J. and Taiebat, M. 2019. Impact of bidirectional seismic shearing on the volumetric response of sand deposits. *Soil Dynamics and Earthquake Engineering*, 125: 105665.

Reyes, A., Yang, M., Barrero, A.R. and Taiebat, M. 2021. Numerical modeling of soil liquefaction and lateral spreading using the SANISAND-Sf model in the LEAP experiments. *Soil Dynamics and Earthquake Engineering*, 143:106613.

Robertson, P.K., et al. 2000. The CANLEX project: summary and conclusions. *Canadian Geotechnical Journal* 37(3): 563-591.

Shahir, H., Pak, A., Taiebat, M. and Jeremić, B., 2012. Evaluation of variation of permeability in liquefiable soil under earthquake loading. *Computers &z Geotechnics*, *40*:74-88.

Taiebat, M., Shahir, H. and Pak, A., 2007. Study of pore pressure variation during liquefaction using two constitutive models for sand. *Soil Dynamics and Earthquake Engineering*, 1(27):60-72.

Taiebat, M. and Dafalias, Y.F. 2008. SANISAND: simple anisotropic sand plasticity model. *International Journal of Numerical and Analytical Methods in Geomechanics* 32(8):915–48.

Taiebat, M., Jeremić, B., Dafalias, Y.F., Kanya, A.M., Cheng, Z. 2010. Propagation of seismic waves through liquified soils. *Soil Dynamics and Earthquake Engineering* 30(4), 236–257.

Tasiopoulou, P., Taiebat, M., Tafazzoli, N. and Jeremic, B., 2015. On validation of fully coupled behavior of porous media using centrifuge test results. *Coupled systems mechanics*, *4*(1):37-65.

Valsamis, A.I., Bouckovalas, G.D. and Papadimitriou, A.G. 2010. Parametric investigation of lateral spreading of gently sloping liquefied ground. *Soil Dynamics and Earthquake Engineering*, 30: 490-508.

Vargas, R.R., Ueda, K. and Uemura, K. 2020. Influence of the relative density and K0 effects in the cyclic response of Ottawa F-65 sand-cyclic Torsional Hollow-Cylinder shear tests for LEAP-ASIA-2019. *Soil Dynamics and Earthquake Engineering*, 133: 106111.

Yang, M., Seidalinov, G. and Taiebat, M., 2019. Multidirectional cyclic shearing of clays and sands: Evaluation of two bounding surface plasticity models. *Soil Dynamics and Earthquake Engineering*, *124*:230-258.

Yang, M., Taiebat, M. and Dafalias, Y.F. 2022. SANISAND-MSf: a sand plasticity model with memory surface and semifluidised state. *Géotechnique*, 72: 227-246

Youd, T., Hansen, C. and Bartlett, S. 2002. Revised multilinear regression equations for prediction of lateral spread displacement. *Journal of Geotechnical and Geoenvironmental Engineering*, 128: 1007-1017.